Journal of Porous Materials (2018) 25:1723–1741
https://doi.org/10.1007/s10934-018-0586-3

An efficient and controllable ultrasonic-assisted microwave route for flower-like Ta(V)–MOF nanostructures: preparation, fractional factorial design, DFT calculations, and high-performance N_2 adsorption

Ghasem Sargazi[1,2] · Daryoush Afzali[3] · Ali Mostafavi[4]

Published online: 17 February 2018

Abstract
With respect to different applications of metal–organic framework (MOF) in the medical, industrial and environmental fields, it is very important to choose a new structure that can be synthesized by fast, eco-friendly and affordable methods with distinctive properties so that the properties could be systematically controlled. In this study, new Ta–MOF nanostructures are synthesized by novel methods of microwave (Mw) and ultrasonic assisted microwave (UAMw) in environmental conditions. The final products are characterized by relevant techniques. Although in the both methods, the synthesized products have favourable properties; the use of the UAMw method would produce samples with distinct features such as high thermal stability of 240 °C, average particle size distribution (PSD) of 23 nm and significant specific surface area (SSA) of 2012 m^2/g. For a better comprehension of the Ta–MOF formation, computational studies are performed using DFT calculations. In order to investigate the effect of the synthesis parameters on different features of the products, the fractional factorial design is used. The results of analysis of variance confirm that the parameters such as Mw power, Mw duration, ultrasonic temperature, ultrasonic power and ultrasonic duration have a significant effect on PSD and SSA of Ta–MOF samples. Due to the fractional factorial design of the experiments, response surface methodology would optimize the probability of producing samples with the small PSD of 15 nm and high SSA of 2588 m^2/g; this desirable amount would provide situations to use these compounds in diverse fields.

Keywords UAMw method · Ta–MOF nanostructure · DFT study · Experimental design

1 Introduction

Metal–organic frameworks (MOFs) are a novel class of porous materials, which have recently been used in various fields due to their unique physico-chemical properties [1]. These materials are prepared by various methods under different conditions. It is highly important to choose a method that makes the synthesis of these materials in environmental conditions possible and manufactures high-yielding products with distinctive properties [2]. The ultrasonic and microwave (Mw) methods have advantages including high-speed production, having reactions in environmental conditions, low cost and eco-friendliness [3, 4]. In these methods, compounds with a variety of structures and different physico-chemical properties are synthesized through controlling synthesis conditions [5]. The use of such effective methods, compared to other conventional methods, for the synthesis of samples results in properties of products to be partly improved. However, in some reports, the MOF-samples have low specific surface area (SSA) and bulk size particles [6, 7]. Due to the benefits of ultrasonic and Mw methods, if the both of methods

✉ Daryoush Afzali
daryoush_afzali@yahoo.com

[1] Department of Nanotechnology Engineering, Mineral Industries Research Center, Shahid Bahonar University of Kerman, Kerman, Iran

[2] Young Researchers Society, Shahid Bahonar University of Kerman, Kerman, Iran

[3] Department of Nanotechnology, Graduate University of Advanced Technology, Kerman, Iran

[4] Department of Chemistry, Faculty of Science, Shahid Bahonar University of Kerman, Kerman, Iran

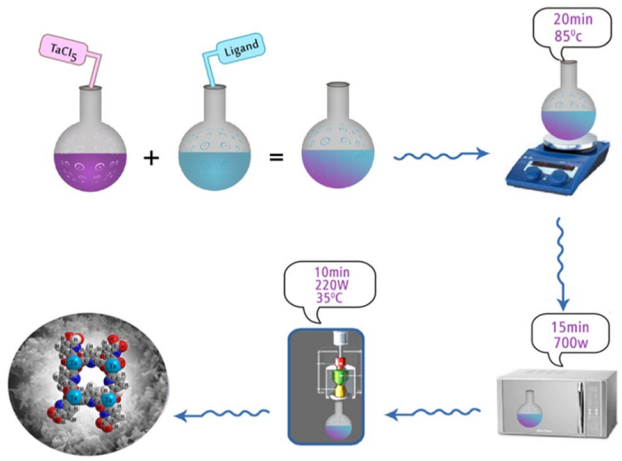

Fig. 1 The schematic representation of Ta–MOF synthesized under optimal conditions of the UAMw method

are used together as a novel method, in which the effects of ultrasonic and microwave parameters on properties of products are systematically studied, we expect the production of samples with more favourable properties. To the best of our knowledge, no study has been conducted on the synthesis of MOFs using an ultrasonic assisted microwave (UAMw) method.

As mentioned earlier, the control of the impact of the synthesis parameters on different properties of MOF-samples is highly important. In previous studies, the effect of several synthesis parameters on properties of products has been examined using conventional designs, in which a number of parameters are assumed constant and one factor is variable. This process not only increases the number of experiments, but also ignores the interaction between parameters [8]. Therefore, the systematic control of products' properties is impossible using conventional designs. In our previous report, the 2^{K-1} factorial design was used to control products' properties [9]. Nevertheless, since a large number of experiments should be selected in this method, it is highly important to choose an ideal design that makes the systematic study of products possible and reduces the number of experiments. The fractional factorial design is one of the systematic ways, through which the number of experiments is reduced and synthesis parameters are scientifically investigated [10]. According to the literatures, no reports have been found on the use of this systematic method for controlling the properties of MOFs.

Many samples of MOFs have been synthesized so far [11, 12]; however, it is important to select and introduce a new

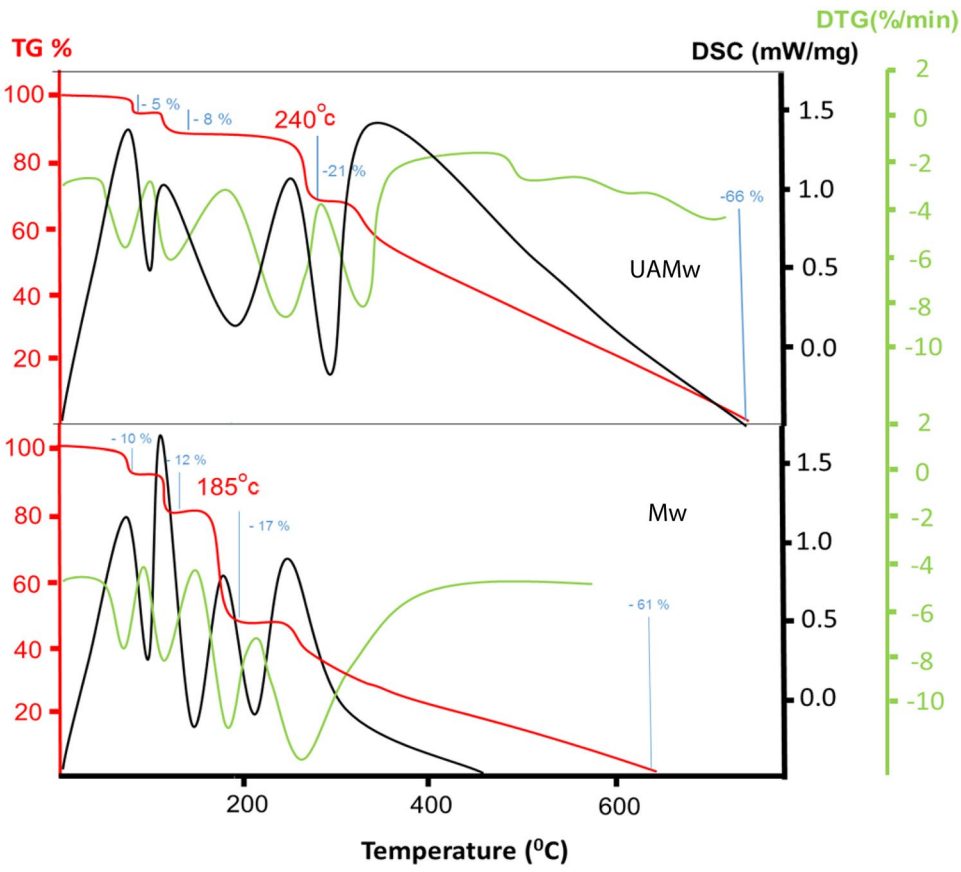

Fig. 2 TGA (red), DSC (black) and DTG (green) curves of the Ta–MOF samples prepared under optimal conditions of the Mw and UAMw method. (Color figure online)

structure, which can draw the attention of researchers for further studies. In our previous study, due to the numerous uses of tantalum nanostructures in industries, electronics and ceramics [13], we synthesized Ta–MOF nanostructure for the first time. In the present study, we decided to synthesize and introduce $C_{21}H_{14}N_3O_{13}Ta$ nanostructure as a new Ta–MOF for manufacturing products with distinctive features using two synthesis methods of Mw and UAMw. To this end, thermogravimetric analysis (TGA), differential scanning calorimetry (DSC), derivative thermogravimetric (DTG) curve, X-ray diffraction (XRD), scanning electron microscopy (SEM), Fourier transform infrared (FT-IR) spectroscopy, CHNS/O elemental analyser, energy dispersive spectrometer (EDS) elemental mapping images, and Brunauer–Emmett–Teller (BET) surface area techniques were used to characterize final products. The Ta–MOF samples were designed using the fractional factorial. For the systematic study of the effect of synthesis parameters on different properties of products, we used analysis of variance and Pareto chart. Finally, response surface methodology (RSM) predicted the possibility of manufacturing products with ideal properties under controlled conditions in the UAMw method.

2 Experimental section

2.1 Materials and instrumentation

Reagent-grade chemicals of tantalum(V) chloride (Mw: 358.21 g/mol, 99.8%), and 2,6-pyridine dicarboxylic acid (Mw: 167.12 g/mol, 99.6%) were purchased from Sigma-Aldrich. All

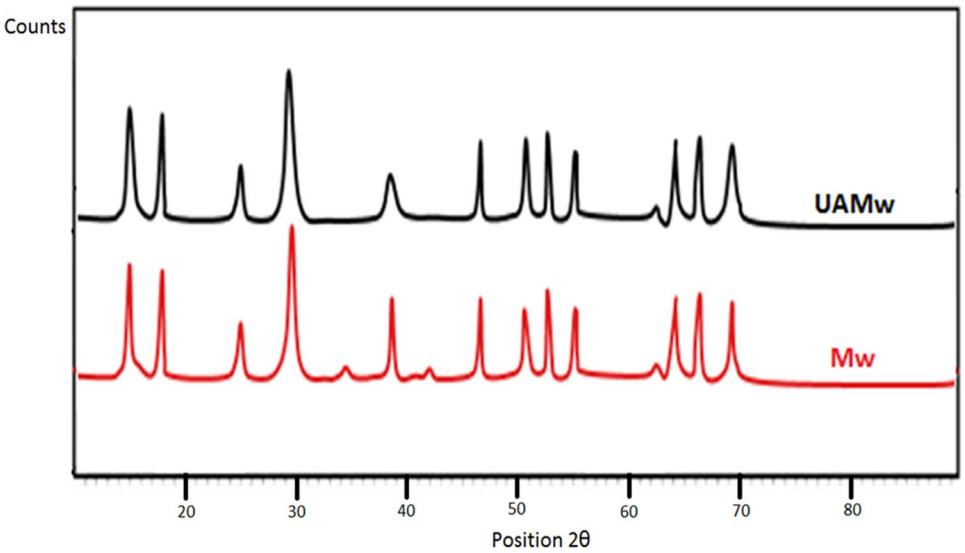

Fig. 3 The XRD patterns of the Ta–MOF samples synthesized by the mean of two different methods (Mw and UAMw)

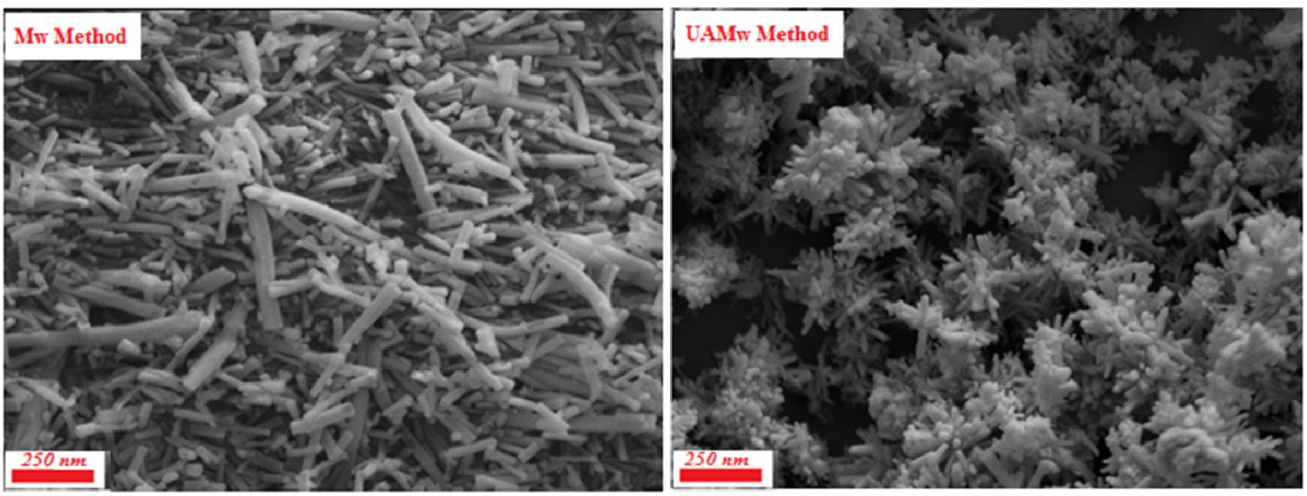

Fig. 4 The SEM images of the Ta–MOF samples synthesized by the Mw and UAMw methods

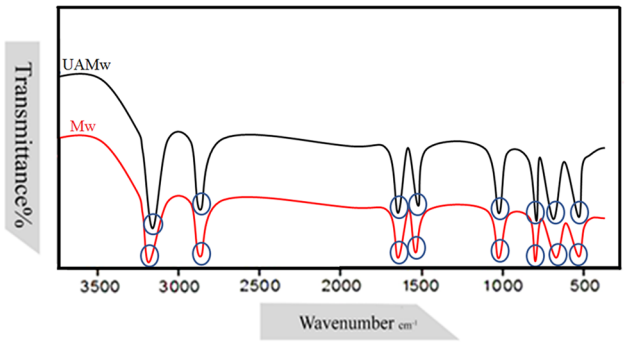

Fig. 5 The FT-IR spectra of the Ta–MOF samples produced by the Mw and UAMw methods

the materials were commercially available and used as received without further purification. TGA (DuPont, TA Q50 analyser), DSC (QMS403C, Netzsch) and DTG (Shimadzu, DTG-60H) were used from room temperature to 800 °C with a heating rate of 5 °C/min under an argon atmosphere. XRD were carried out on Scintag X1 diffractometer with monochromatized CuKα irradiation (λ = 0.1540 nm) in 2θ angles ranging from 10 to 90 °C to collect the crystallographic information. The microscopic features of the Ta–MOF samples were examined using SEM (Nova NanoSEM230). For FT-IR spectroscopy, Thermo Scientific Nicolet-6700 spectrometer was used. CHN/S and EDS elemental mapping images were used to carry out the elemental analysis. BET surface areas of the Ta–MOF samples were determined using a Micromeritics, TriStar II 3020 analyser at 77 K.

2.2 Synthesis of Ta–MOF samples

2.2.1 Microwave (Mw) method

In a typical Mw synthesis, 0.0716 g of $TaCl_5$ (0.2 mmol) and 0.1003 g of pyridine-2,6-dicarboxylic acid (0.6 mmol) were

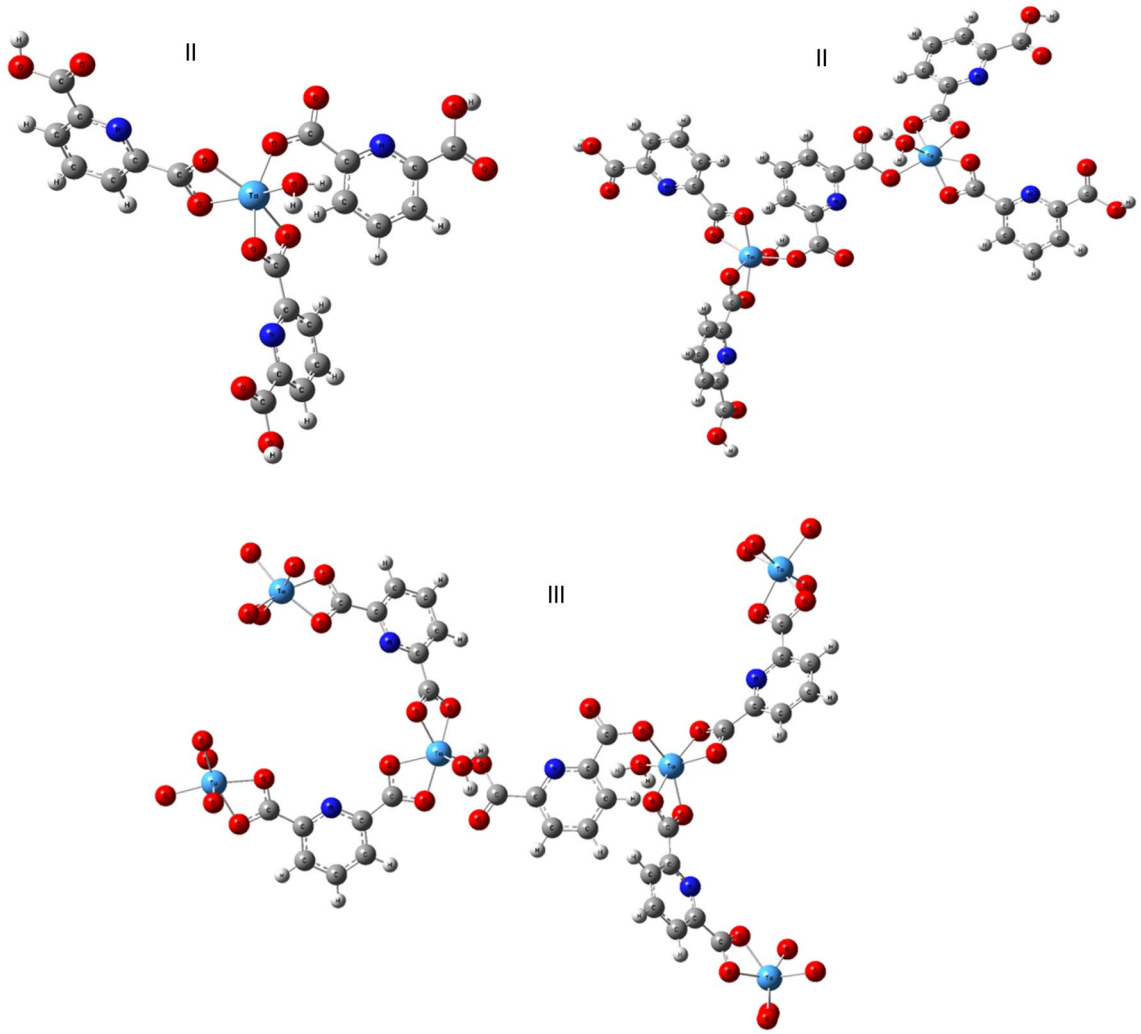

Fig. 6 Representations of the compound ***I*** (as an independent unit), and compounds ***II*** and ***III*** (as expanded units) predicted based on the results of the FT-IR spectrum (color: C: black; N: blue; O: red; Ta: light blue and H: white). (Color figure online)

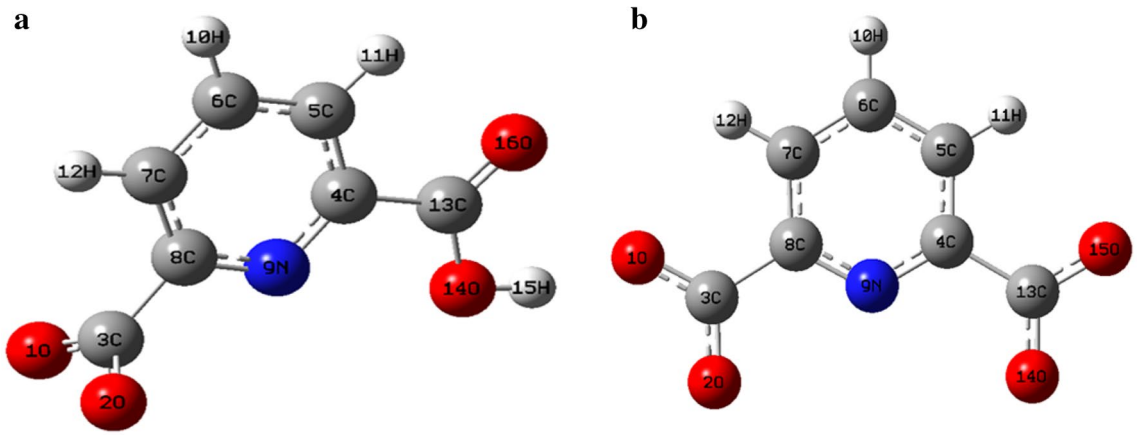

Fig. 7 Representations of the ligand ***A*** (used in the compounds ***I*** and ***II***) and ligand ***B*** (used in the compounds ***II*** and ***III***)

dissolved in 30 mL double-distilled water, and the mixture was stirred approximately 20 min at 85 °C. Then, the compound was put into the Mw reactor and placed under the optimal irradiation with the microwave power of 700 W for 15 min at the ambient temperature.

2.2.2 Ultrasonic assisted microwave (UAMw) method

The synthesis of Ta–MOF nanomaterials using the UAMw method was performed as follows: the mixture, which was obtained in the previous section by microwave irradiation (Sect. 2.2.1), was entered into the ultrasonic bath with the frequency of 20 Hz, undergoing optimal ultrasonic irradiation with the power of 220 W for 10 min at 35 °C. After cooling to room temperature, the products were isolated by washing with distilled water. A simple schematic representation of the synthesis of Ta–MOF is shown in Fig. 1.

Table 1 DFT calculations of the ligand ***A*** used in the compounds ***I*** and ***II***

Method	B3LYP/6-311G	B3LYP/6-31G
Dipole moment (debye)	4.3486	4.3771
Amount of charge on oxygen atoms		
O_1	−0.351	−0.313
O_2	−0.261	−0.220
O_{14}	−0.522	−0.528
O_{16}	−0.403	−0.361
Bond length (angstrom)		
C_3–O_1	1.26942	1.26500
C_3–O_2	1.31103	1.31350
C_{13}–O_{14}	1.36324	1.36257
C_{13}–O_{16}	1.23930	1.23669
Angle		
O_1–C_3–O_2	113.77759	113.84765
O_{14}–C_{13}–O_{16}	122.83087	122.81197
Compound energy (a.u)	−624.71012602	−624.54732499

Table 2 DFT calculations of the ligand ***B*** used in the compounds ***II*** and ***III***

Method	B3LYP/6-31G	B3LYP/6-311G
Dipole moment (debye)	4.0702	8.287
Amount of charge on oxygen atoms		
O_1	−0.13	−0.301
O_2	−0.102	−0.277
O_{14}	−0.102	−0.277
O_{15}	−0.13	−0.301
Bond length (angstrom)		
C_3–O_1	1.31801	1.25478
C_3–O_2	1.32343	1.30725
C_{13}–O_{14}	1.32343	1.30726
C_{13}–O_{15}	1.31801	1.25478
Angle		
O_1–C_3–O_2	112.90728	121.12259
O_{14}–C_{13}–O_{15}	112.90916	121.12258
Compound energy (a.u)	−615.75902	−623.97981

3 Results and discussion

3.1 Thermodynamic behaviour

Thermodynamic behaviour of the Ta–MOF samples synthesized using the Mw and UAMw methods is shown in Fig. 2. Based on the results obtained from TGA, the thermal behaviour of the samples in both the methods would follow a certain pattern and the Ta–MOF samples would suffer from weight loss in four steps [14]. The first step can be attributed to the evaporation of adsorbed water. In the second step, the trapped water in the structure is decomposed. After this step, the pure product of Ta–MOF

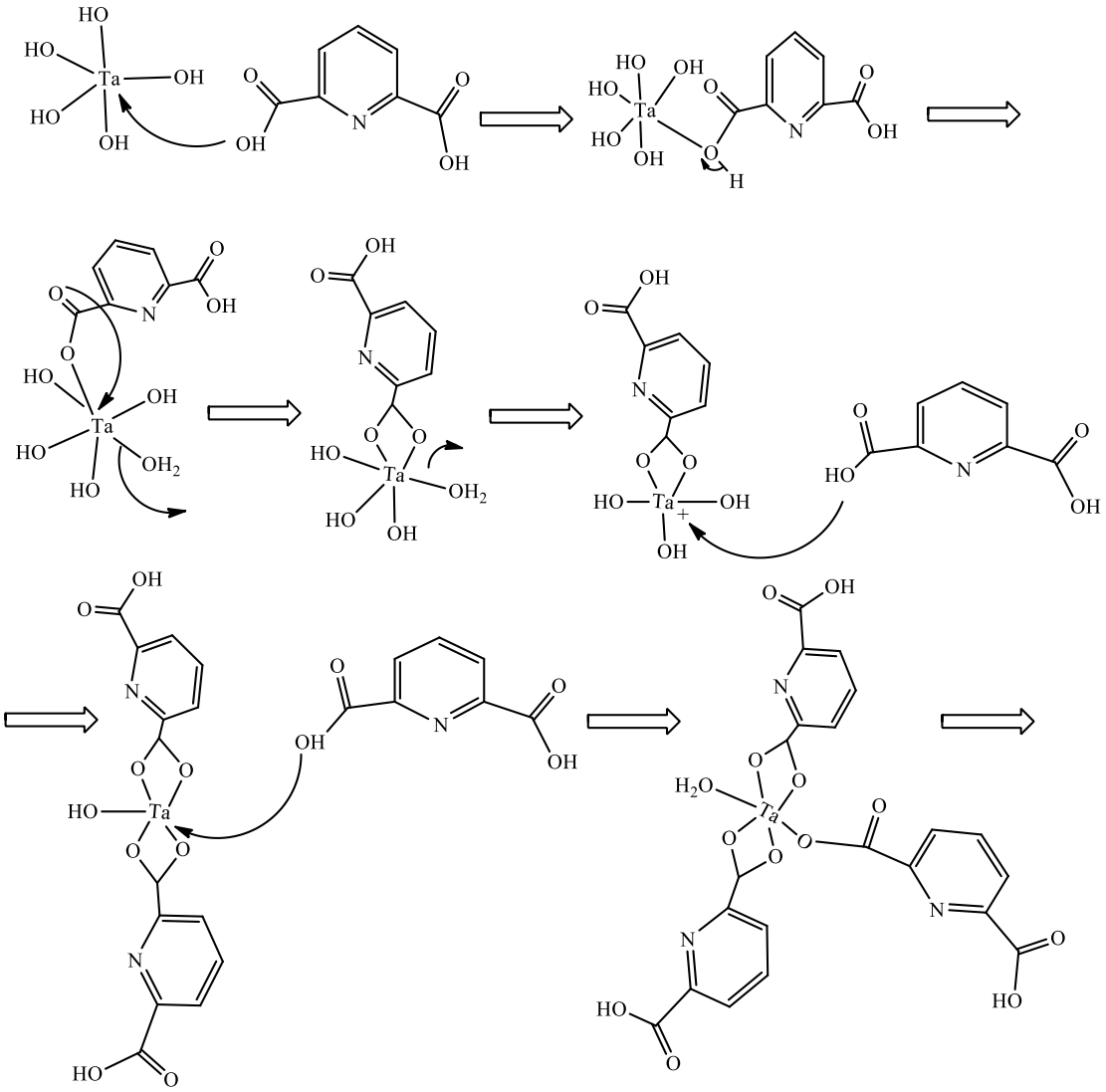

Fig. 8 The proposed mechanism of the Ta–MOF samples synthesized under optimal conditions of the Mw and UAMw methods

is obtained. In the third step, in both the samples, there is significant weight loss, and the structure of the MOFs is degraded. In the final step, the residual components of the samples are disintegrated. The results show that the use of the UAMw method would produce samples with higher thermal stability (240 °C in the UAMw method compared to 185 °C in the Mw method). Since the pure product obtained contains 87% of the initial sample weight in the UAMw method, while it contains 78% of the initial sample weight in the Mw method, it is concluded that the UAMw method, compared to the Mw method, would produce higher-yielding samples. DSC and DTG analyses approve the results of TGA, representing that the thermodynamic behaviour of the Ta–MOF samples is in four distinct steps and each step requires particular energy [9].

3.2 Crystallinity

Figure 3 shows the XRD patterns of the Ta–MOF samples with high crystallinity, which are synthesized using the Mw and UAMw methods. Although based on Debye–Scherrer equation, the crystal size of both the samples is in the nanometric range [15], the sample synthesized by the UAMw method has smaller crystal size for having wider peaks (22 nm in the UAMw method compared to 56 nm in the Mw method). Since the samples are synthesized in two different conditions, it is possible that the synthesis parameters would have a great effect on the size of crystals. In both the Mw and UAMw methods, the corresponding XRD patterns were indexed to the monoclinic crystal system of the pure complex of $C_{21}H_{14}N_3O_{13}Ta$ with the space group *P21/n* and unit

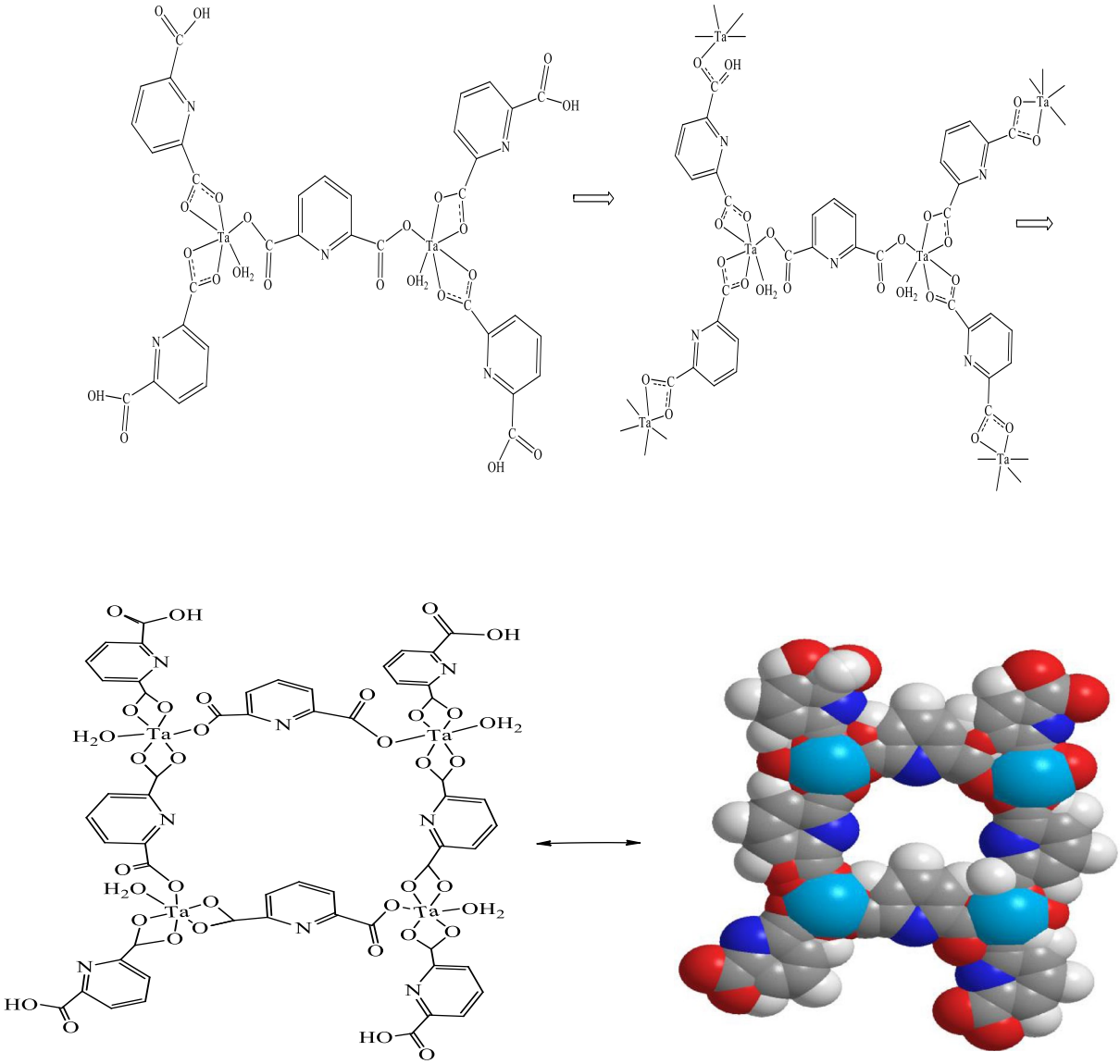

Fig. 8 (continued)

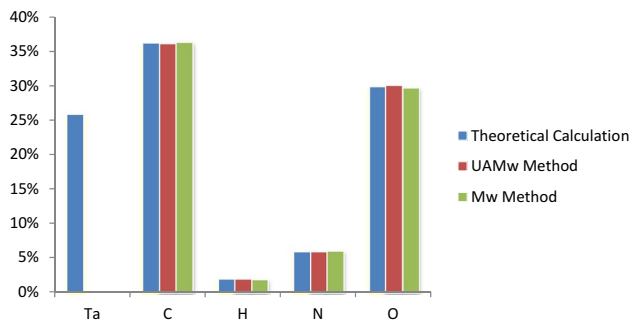

Fig. 9 The CHNS/O elemental analysis for the Ta–MOF samples synthesized under optimal conditions (the theoretical calculation: blue, the UAMw method: red and the Mw method: green). (Color figure online)

cell parameters of a = 12.986 Å, b = 8.9104 Å, c = 24.942 Å, and α = 90.049.

3.3 Morphology and size distribution

Figure 4 demonstrates the SEM images of the Ta–MOF samples synthesized under optimal conditions of the Mw and UAMw methods. Based on the results, the morphology of the sample synthesized by the Mw method is rod-shaped with the average diameter of 76 nm; however, using the UAMw method would produce nanoparticles with flower-like morphology. The sample synthesized by the UAMw method has more uniform morphology than that synthesized by the Mw method; accordingly, no evidence of agglomeration and aggregation of particles can be found while using

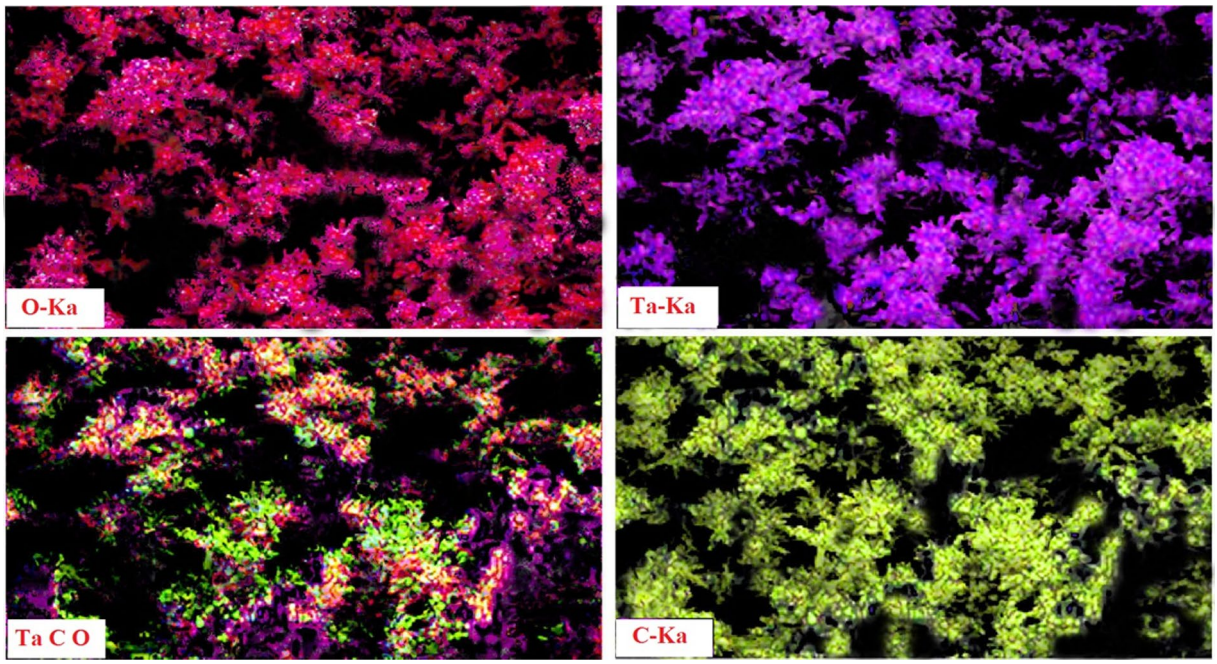

Fig. 10 The EDS elemental mapping images for the Ta–MOF samples synthesized under optimum condition of the Mw and UAMw methods

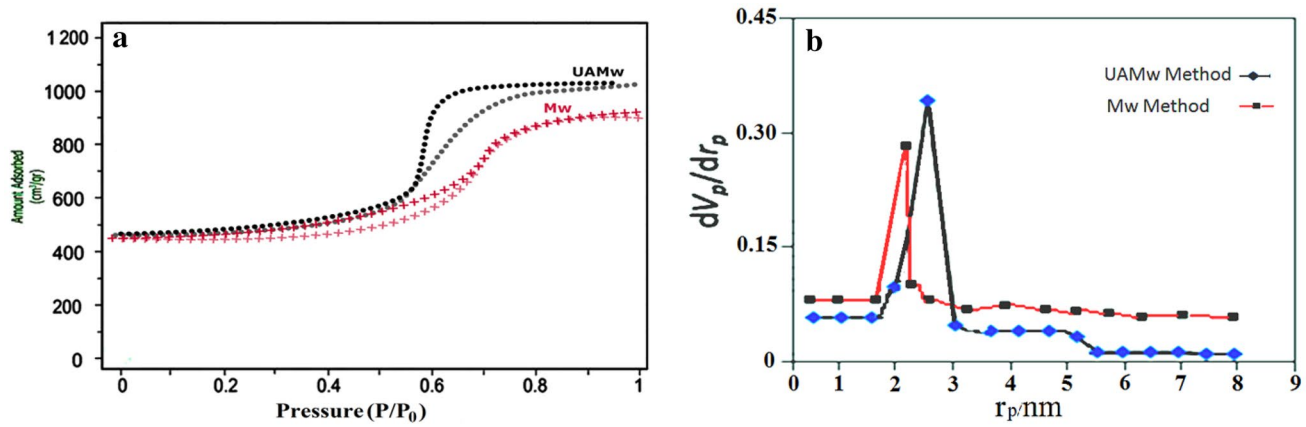

Fig. 11 The N_2 adsorption/desorption isotherms (**a**) and pore size distribution (**b**) of the Ta–MOF samples synthesized under optimal conditions of the Mw and UAMw methods

Table 3 Coded and non-coded levels of the UAMw parameters based on the fractional factorial design

Level	Coded level	Non-coded level				
		Microwave power (W)	Microwave duration (min)	Ultrasonic temperature (°C)	Ultrasonic power (W)	Ultrasonic duration (min)
High	+1	900	20	45	320	15
Center	0	700	15	35	220	10
Low	−1	500	10	25	120	5

Coded formula: $\frac{x-\frac{x\ (high)+x(low)}{2}}{\frac{x(\ high)-x(low)}{2}}$, x : $-w \ldots, -3, -2, -1, 0, 1, 2, 3, \ldots . +w$

Table 4 Randomized complete fractional factorial designs for different experimental conditions of the Ta–MOF samples synthesized by the UAMw method

Sample (Condition)	Std order	Center Pt	A (W)	B (min)	C (°C)	D (W)	E (min)	REP	PSD (nm)	SSA (m^2/g)	Morphology
a	9	1	0	−1	+1	−1	−1	1	153	1190	Rod-shaped microstructure
								2	155	192	
b	5	1	−1	0	0	−1	0	1	45	1820	Spherical nanostructure
								2	44	1818	
c	6	1	−1	−1	−1	0	0	1	108	1420	Flower-like microstructure
								2	108	1419	
d	3	1	0	0	0	0	0	1	23	2012	Flower-like nanostructure
								2	23	2012	
e	2	1	−1	−1	−1	−1	−1	1	921	322	Bulk structure
								2	918	321	
f	8	1	0	0	0	−1	0	1	30	1978	Rod-shaped nanostructure
								2	30	1976	
g	4	1	+1	+1	+1	+1	+1	1	984	212	Bulk structure
								2	980	211	
h	7	1	+1	0	+1	+1	0	1	204	742	Spherical microstructure
								2	204	740	

PSD Particle size distribution, *SSA* Specific surface area

the UAMw method. However, in the Mw method, the particles are partially aggregated, which can increase the diameter of the Ta–MOF sample.

3.4 Chemical composition

Figure 5 demonstrates the FT-IR spectra of the Ta–MOF samples that have been synthesized by the Mw and UAMw method under optimal condition. In the both spectra, the absorption peak near 3198.44 cm^{-1} is related to the coordinated water in the structure. The frequency observed at 2847.12 cm^{-1} confirms the presence of the stretching vibrations of aromatic CH. The absorption peaks near 1605.33 and 1564.47 cm^{-1} can be assigned to the –COO– groups, and the frequency absorption near 1014.94 cm^{-1} is ascribed to the C–N bond. The absorption band at 874.06 cm^{-1} is due to the C–H bending vibrations, and the frequencies around 782.29 and 702.57 cm^{-1} are assigned to the Ta–O bond.

According to the results of the FT-IR spectra and with regard to various configurations of ligand, the compound ***I*** was predicted as the independent unit and the compounds ***II*** and ***III*** were predicted as the expanded units (Fig. 6). In order to determine the structural stability of the compounds, the density functional theory (DFT/B3LYP) method coupled with 6-31G and 6-311+G functionals were utilized [16]. Since ligands are the base of expansion of structures (Fig. 7), the stability of ligands was examined to determine which of these compounds were stable. The structural information of these ligands, which was obtained using the theoretical methods, is reported in Tables 1 and 2. According to the results, in both the B3LYP/6-31G and B3LYP/6-311G methods, the ligand ***A*** had less energy than the ligand ***B***. Since the compounds ***I, II*** and ***III*** were respectively made of the ligand ***A***, ligands ***A*** and ***B***, and ligand ***B***, it can be concluded that the compound ***III*** is more stable because it is made of a ligand with less energy. Moreover, since the ligand attacks the metal with its head (OH) and forms a complex, the probability of complex stability is higher in the structures, in which the charge density on oxygen is low. Table 2 shows that the charge density on oxygen atoms is low in the compound ***III***, which implies the stability of this structure. The results of the theoretical methods approve the formation of the compound ***III*** as a piece of evidence for the expansion of the primary units. Therefore, this issue strengthens the formation of a MOF with a polymeric structure. The proposed mechanism as well as the final structure of the formation of Ta–MOF is presented in Fig. 8.

The amounts of carbon, hydrogen, nitrogen and oxygen, which were obtained by the experimental methods using CHNS elemental analysis, as well as the results of theoretical computations are shown in Fig. 9. As can be observed, the results of elemental analysis in both the experimental methods of Mw and UAMw are consistent with theoretical calculations. These results confirm the final structure related to the proposed mechanism of the Ta–MOF ($C_{21}H_{14}N_3O_{13}Ta$) shown in Fig. 8. In order to understand the origin of the structure morphology, EDS elemental mapping images were applied on the Ta–MOF sample synthesized by the UAMw

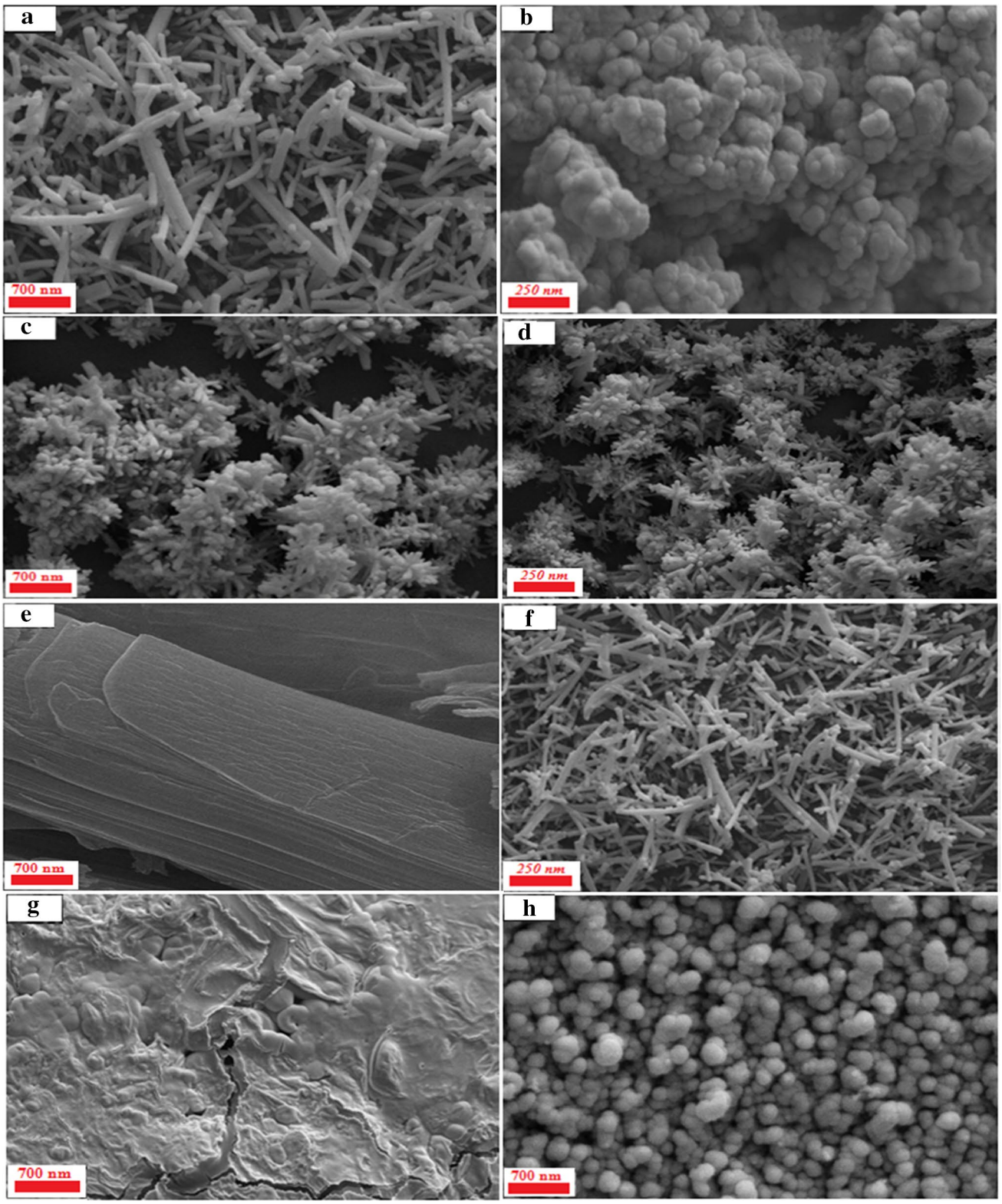

Fig. 12 The SEM images of the Ta–MOF samples synthesized under different conditions of the UAMw method (**a**–**h**)

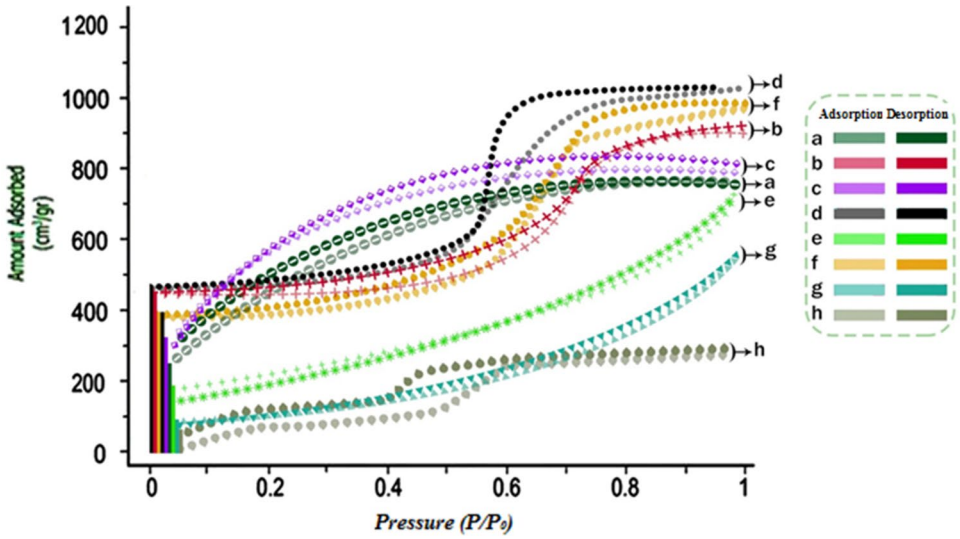

Fig. 13 The N_2 adsorption/desorption isotherms of the Ta–MOF samples synthesized under different conditions of the UAMw method (*a–h*)

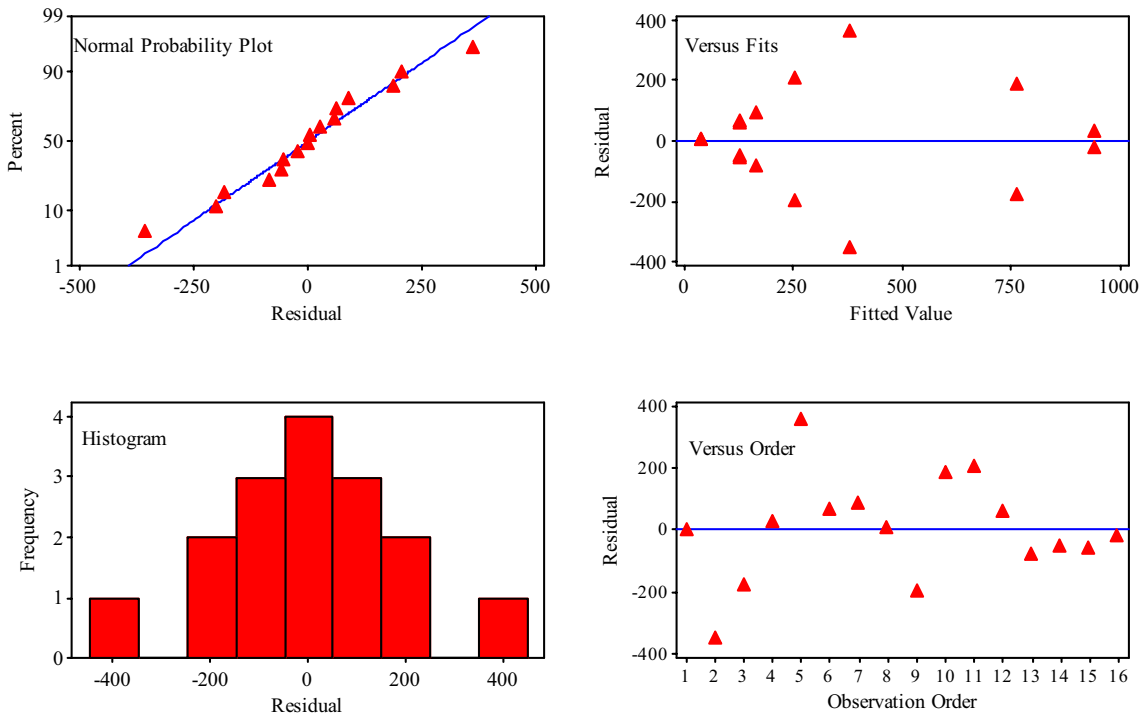

Fig. 14 Normal probability plots of the residuals for PSD results

method. According to Fig. 10, the flower-like morphology of this nanostructure was due to the presence of Ta, O and C elements; besides, the CHNS elemental analysis confirmed the presence of these elements in the structure.

3.5 Textural properties

The nitrogen adsorption/desorption isotherms of the products synthesized by the methods of Mw and UAMw are shown in Fig. 11a. According to the IUPAC classification of adsorption/desorption isotherms [17, 18], although the Ta–MOF samples produced by both methods have a mesoporous nature, based on the results of BET surface area technique, the sample synthesized by UAMw method has a higher SSA (2012 m^2/g in the UAMw method than 1784 m^2/g in the Mw method). Figure 11b also shows the pore size distribution of the samples based on the BJH method in both the experimental MW and UAMW methods; as can be seen, the mean pore size distribution of the

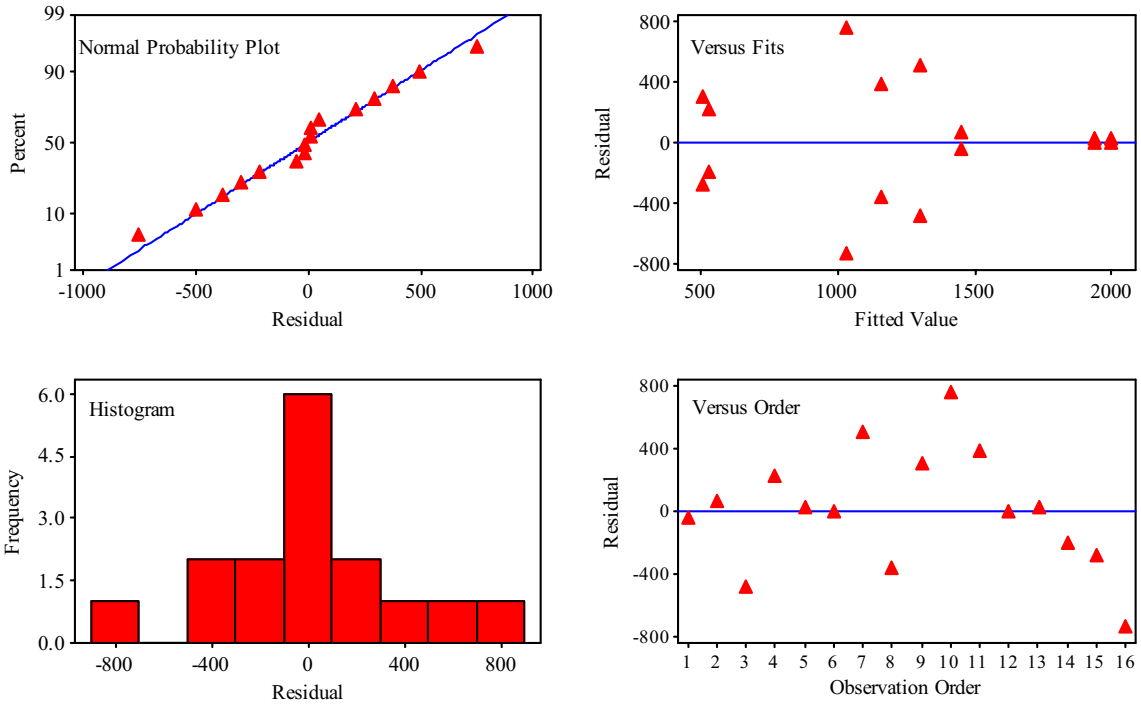

Fig. 15 Normal probability plots of the residuals for SSA results

Table 5 Analyses of variance for PSD and SSA of the Ta–MOF samples synthesized under different conditions of the UAMw method

Source	Adj MS		F_{value}		P_{value}	
	PSD	SSA	PSD	SSA	PSD	SSA
A	210.21	324.47	8547.48	7458.32	0.000	0.000
B	144.47	297.98	7145.49	6599.45	0.006	0.008
C	89.69	146.37	7046.65	6480.98	0.009	0.008
D	64.25	97.74	6547.35	5898.20	0.009	0.013
E	50.30	74.36	5784.61	4990.39	0.012	0.018
AB	32.87	64.77	3025.54	3578.08	0.016	0.021
AC	13.45	46.54	1640.48	2021.40	0.020	0.028

R^2: 99.96%; R^2(pred): 99.89%; R^2(adj): 99.87%

Ta–MOF samples is 2.6 nm in the UAMw method and 2.1 nm in the Mw method.

3.6 Experimental design

Several characterization techniques indicated that although the Ta–MOF samples synthesized by the Mw and UAMw methods had desirable properties, the use of the UAMw method yielded products with higher efficiency and more desirable properties such as higher thermal stability, higher surface area and more uniform morphology. Therefore, this route was selected as the ideal method and employed in the design of the experiment. Since conventional experimental designs result in increased number of experiments and also, do not taken into account the interaction between factors, in case of using these conventional methods, it would not be possible to systematically investigate the effect of synthesis parameters on different properties of products [19]. Accordingly, the scientific experimental design known as fractional factorial design was used in the present study. The fractional factorial range is very critical problem to seek an optimization. At first, we used the experimental condition reported in previous similar works [9, 20]. At last, using XRD, TG/DSC, FTIR and SEM we could find that how theses selected parameters could influence drastically on the final structure and properties of material synthesized by this method. In this scientific design, the synthesis parameters of the UAMw method, including Mw power (A), Mw duration (B), ultrasonic temperature (C), ultrasonic power (D) and

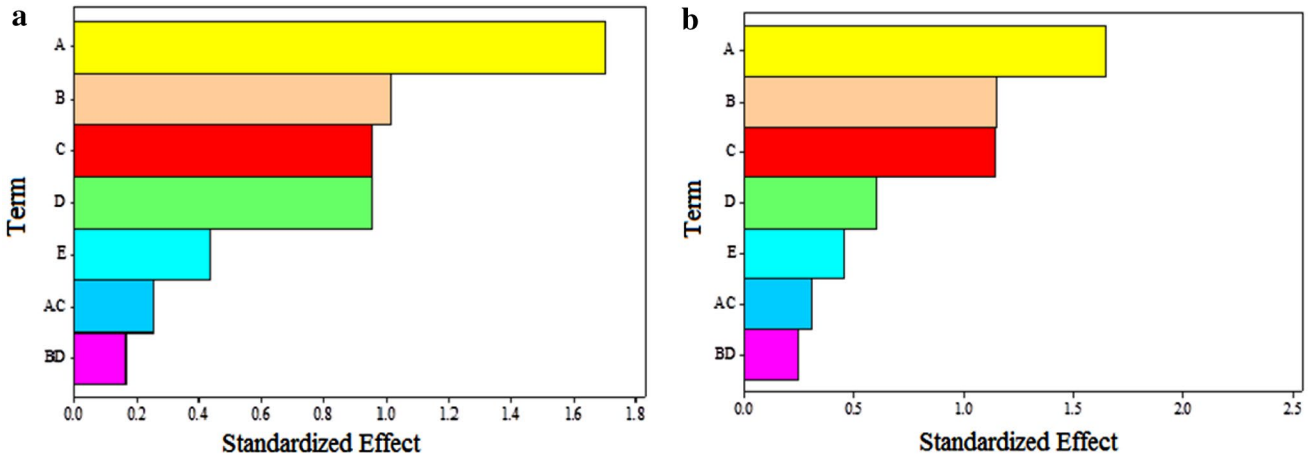

Fig. 16 The Pareto charts of the effect of the synthesis parameters on properties of the Ta–MOF samples

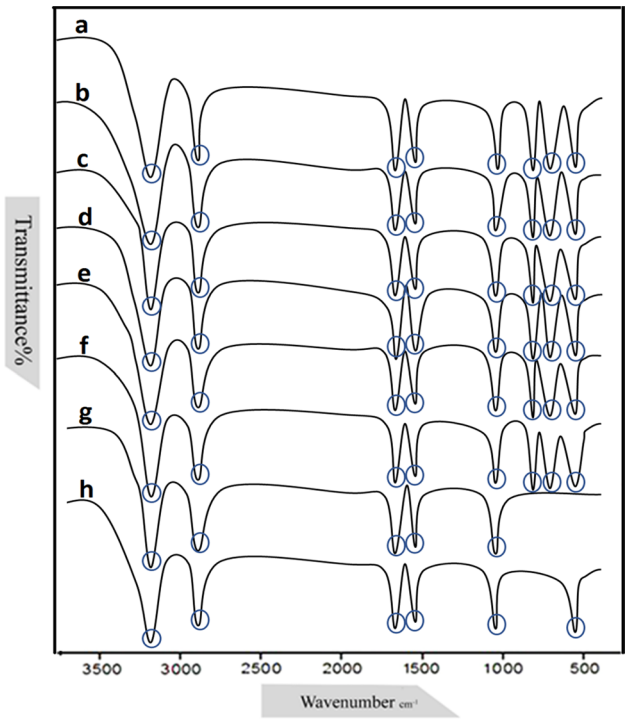

Fig. 17 The FT-IR spectra of the Ta–MOF samples synthesized under different conditions of the UAMw method (*a–h*)

ultrasonic duration (E) were selected. Then, effects of these parameters on the properties of the Ta–MOF sample such as their particle size distribution (PSD) and SSA were studied. Coded levels of each parameter were considered equal to +1, 0 and −1 (Table 3). Then, several experiments were designed using this method. The design matrix and response data obtained from two replicates of the experiments are shown in Table 4 (18 runs were made in a random order). In contrast to other conventional methods, in which parameters in each experiment are considered constant and only one parameter is considered variable in order to investigate effect of that variable parameter, the parameters in the fractional factorial design were assumed variable [21, 22].

Figure 12 shows the SEM image of the Ta–MOF samples synthesized in different conditions of the synthesis parameters of the UAMw method, which had been designed via fractional factorial. Based on the data obtained from these images, depending on the synthesis conditions, the Ta–MOF samples had various morphologies. Besides, their mean PSD was different so that the sample ***d*** was selected as the optimal sample due to having a smaller PSD than the other samples. Figure 13 shows the N_2 adsorption/desorption isotherms of the Ta–MOF samples synthesized in different conditions of the UAMw method, including microwave parameters (power and duration) and ultrasonic parameters (temperature, power and duration). As can be observed in this Figure, the samples exhibited various adsorption/desorption behaviours; furthermore, based on the data obtained from the BET technique, these samples (a–h) had different SSAs in different synthesis conditions. A comparison between different synthesis conditions indicated that the condition ***d***, in which the sample had maximum SSA, could be considered as the optimal condition. The obtained results indicated that properties of the Ta–MOF samples obtained in the present study were significantly improved compared to those of other MOF samples that had been previously synthesized through different methods and under different synthesis conditions [23–26]. Moreover, the thermal stability (240 vs. 218 °C), mean PSD (23 vs. 73 nm) and SSA (2012 vs. 1940 m^2/g) of the Ta–MOF sample, which were synthesized by the UAMw method in optimal conditions in the present study, were improved compared to those of the

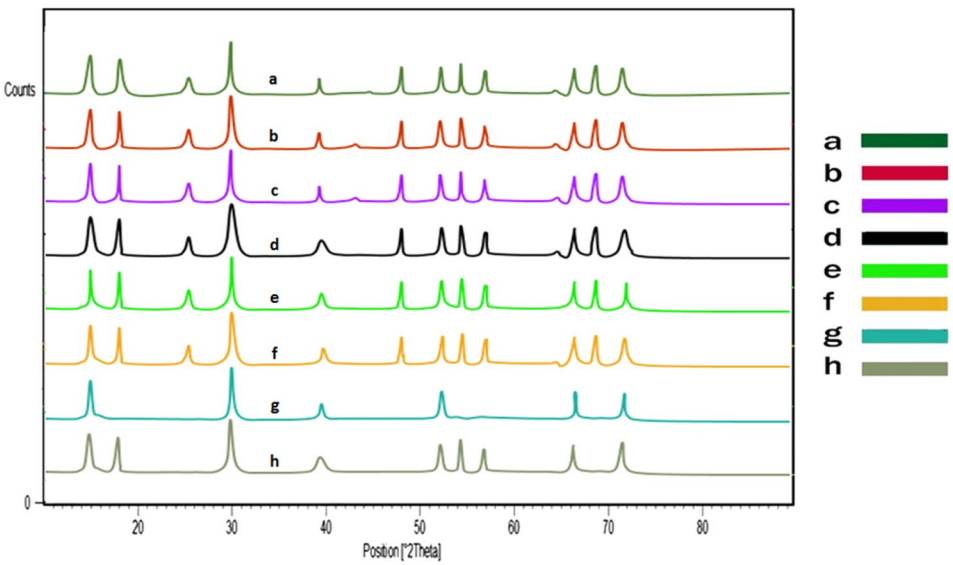

Fig. 18 The XRD patterns of the Ta–MOF samples synthesized under different conditions of the UAMw method (*a–h*)

previous sample synthesized using ultrasonic method [9]. Such improvement could be attributed to the type of the synthesized compound, application of the optimal synthesis conditions and use of a novel synthesis method since the UAMw method was employed in the present study.

3.7 Ultrasound assisted microwave (UAMw) effects

To ensure that the design of the experiments is scientific and probability distribution is normal, the residual plots for the results of PSD and SSA of the Ta–MOF samples synthesized in different UAMw conditions are shown in Figs. 14 and 15. It is clear that, in all types of residual plots for every property, the number of positive and negative levels is equal, which is compelling evidence for the scientific design and normal distribution of the experiments [27, 28].

Analysis of variance (ANOVA) was employed to study the effect of UAMw parameters on the PSD and SSA of the Ta–MOF samples. To interpret the results of ANOVA, $\boldsymbol{\alpha}_{value}$ and $\boldsymbol{p}_{value}$ belonging to each factor were compared together [29, 30]. The $\boldsymbol{\alpha}_{\mathbf{value}}$ (standard significance level) was set to 0.05 by default. The $\boldsymbol{P}_{value}$ ($\boldsymbol{P}_{value}$ is a number between 0 and 1, and used to weigh the strength of the data validity) varies according to the magnitude of the effect of synthesis parameters on sample properties [31]. The effect of a parameter on the properties in question is revealed if $\boldsymbol{P}_{value}$ is smaller than $\boldsymbol{\alpha}_{value}$ for that parameter. Based on the ANOVA results in Table 5, the parameters of Mw power (A), Mw duration (B), ultrasonic temperature (C), ultrasonic power (D) and ultrasonic duration (E) have a small $\boldsymbol{P}_{value}$ (equal or close to 0.0). Thus, all these parameters have significant effects on the PSD and SSA of the Ta–MOF samples. Moreover, small $\boldsymbol{P}_{value}$ in ***AC*** and ***BD*** inactions confirms that the interaction between ultrasonic and Mw parameters affects the properties of the Ta–MOF products. The magnitude of the effect of synthesis parameters and the interaction among them is illustrated using Pareto charts in Fig. 16.

In the present study, the Ta–MOF samples had various PSDs, morphologies and SSAs depending on the synthesis conditions. The results of ANOVA and Pareto charts showed that the parameters of Mw power, microwave duration, ultrasonic temperature, ultrasonic power and ultrasonic duration had significant effects on these properties. Regarding the systematic studies, the sample ***d*** was selected as the optimal sample, and values of the parameters of the UAMw method, which led to the synthesis of this sample with desirable properties, were selected as the optimal value. These synthesis parameters, which are a combination of parameters of the microwave and ultrasonic methods, yielded the Ta–MOF nanostructure (the sample ***d***) with uniform morphology, flower-like structure and average PSD of 23 nm (Fig. 12d). According to the IUPAC classification, the sample ***d*** had behaviour similar to that of the fifth type of the N_2 adsorption/desorption isotherms series, indicating the meso-size distribution of the pores (Fig. 13d). Furthermore, results of the BET technique showed that the surface area of this sample was higher than that of other samples.

Figure 17 shows the FT-IR spectra of the Ta–MOF samples synthesized under different conditions of the UAMw method (a–h). Accordingly, at the conditions ***g*** and ***h***, no bonds related to the formation of Ta–O were observed; thus, it can be concluded that in the samples ***g*** and ***h***, the Ta–MOF bonds were not formed properly; however, in the other samples, all the bonds related to the formation of Ta–MOF can be observed. Since at the conditions ***g*** and ***h***, some of the synthesis parameters had higher intensity than the optimal parameters, such high

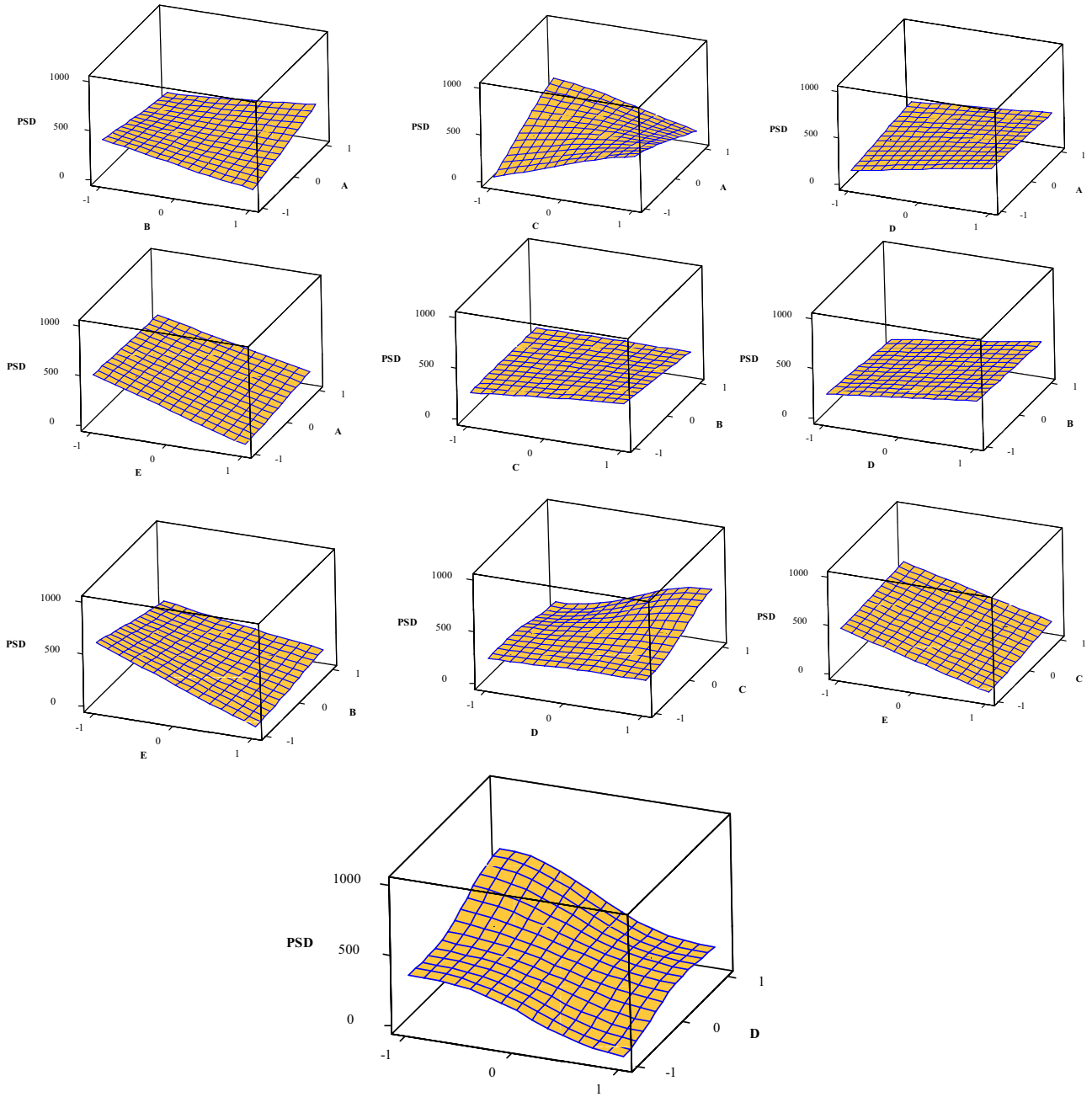

Fig. 19 Surface plots for PSD of the Ta–MOF samples obtained from a regression model

intensity could cause destruction of the bonds related to the formation of MOF, which would result in the synthesis of the samples with bulk-range PSD (Fig. 12g, h). Moreover, the interaction between the ultrasonic and microwave parameters, the effect of which was confirmed by ANOVA, would increase the intensity of such destruction. Thus, at the condition ***g***, in which all the microwave and ultrasonic synthesis parameters were at their highest intensity compared to the optimal condition, the sample's adsorption behaviour (Fig. 13g) was similar to that of the third type of the adsorption isotherms (the behaviour of the nonporous systems) [17, 32]. However, at the condition ***h***, in which the parameters of microwave power, ultrasonic temperature and ultrasonic power were at their highest levels and the other synthesis parameters were in their optimal condition, the N_2 adsorption behaviour of the sample ***h*** was similar to that of the second type of the isotherms, indicating the irregular interaction between the adsorbent and adsorbate (Fig. 13h) [33]. In the samples ***e*** and ***a***, based on the FT-IR, although all the bonds related to

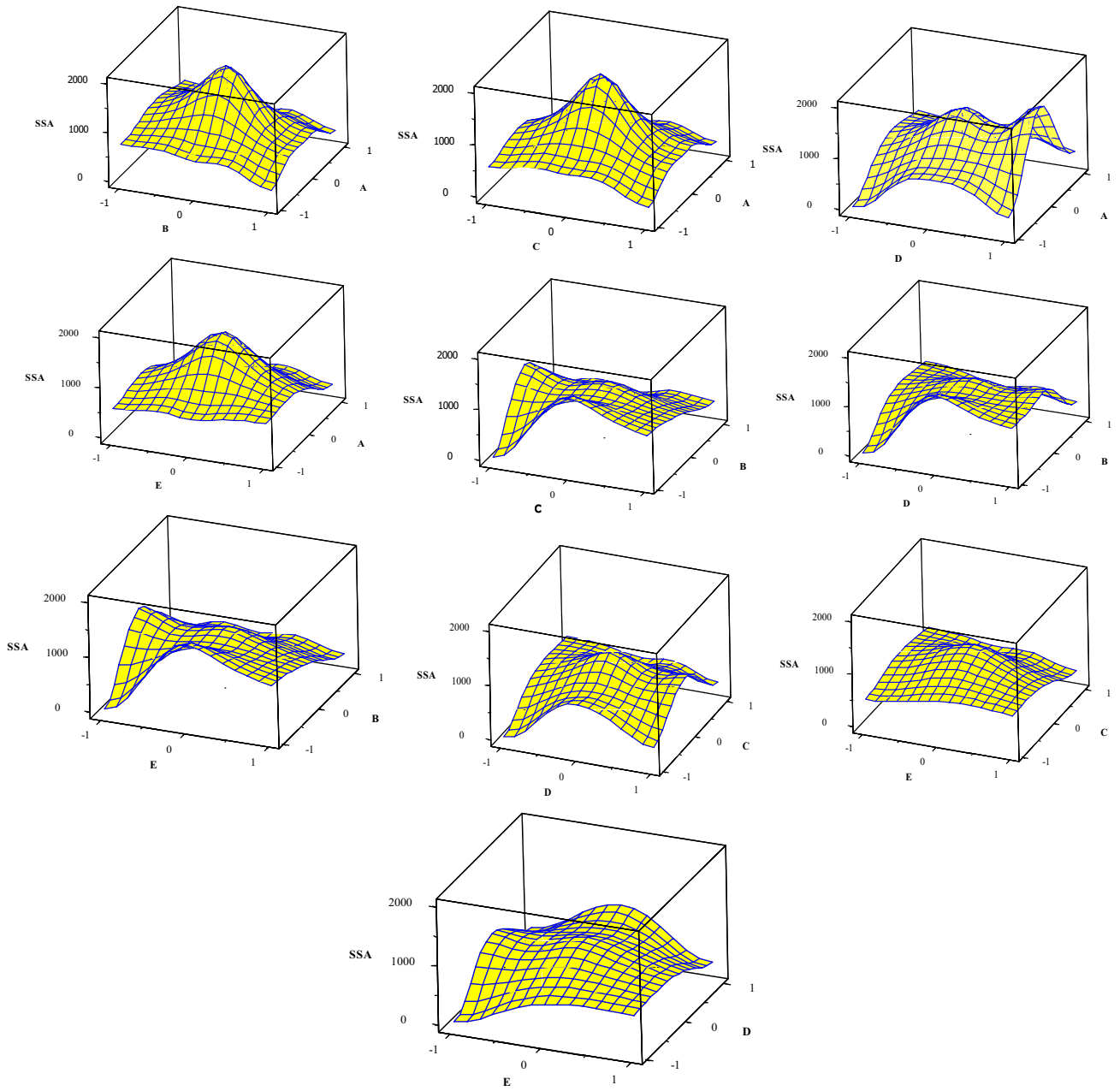

Fig. 20 Surface plots for SSA of the Ta–MOF samples obtained from a regression model

the formation of Ta–MOF were formed properly, selection of the synthesis parameters at their lowest level at the condition ***e*** compared to the optimal conditions led to the agglomeration of the particles as well as their bulk-range size distribution (Fig. 12e). Furthermore, the N_2 adsorption behaviour of the sample ***e*** was due to the nonporous system so that the SSA of this sample was considerably reduced (Fig. 13e). However, at the condition ***a***, since the parameters of microwave duration, ultrasonic power and ultrasonic duration were selected at their lowest levels compared to the optimal conditions and only the parameter of microwave power had an optimal value, morphology of the sample ***a*** was in a microstructure rod-shaped form (Fig. 12a). Moreover, its adsorption/desorption isotherm was similar to that of the first type of the isotherms, indicating the microporous nature of the pores (Fig. 13a) [20]. In the samples ***c, f*** and ***b***, depending on the extent to which the synthesis parameters were close to the optimal parameters' values, the morphology, N_2 adsorption/desorption behaviour and PSD of the samples were different. Table 4

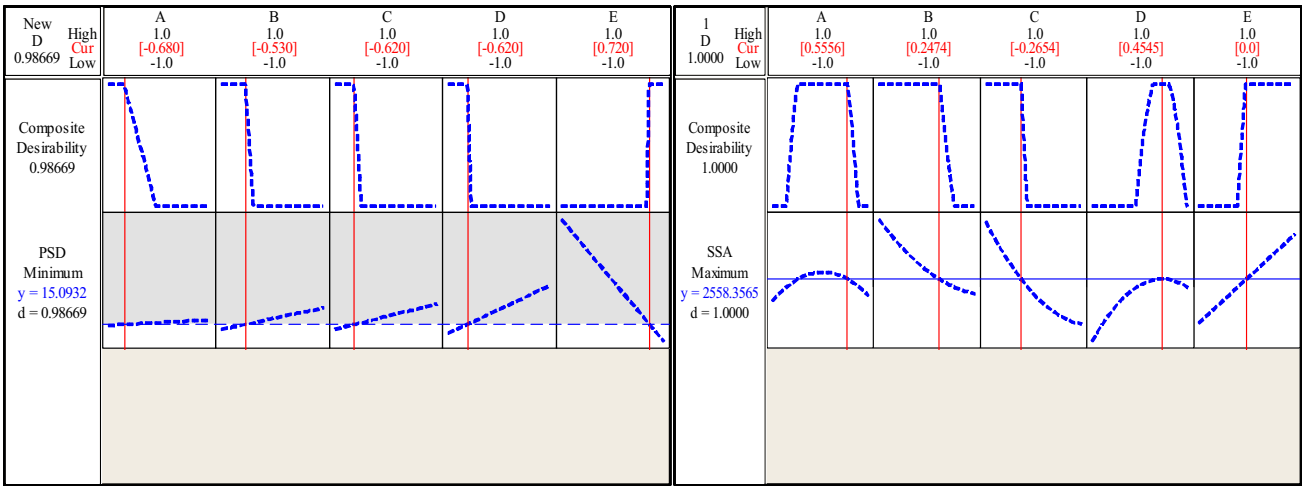

Fig. 21 RSM plots for PSD and SSA of the Ta–MOF samples

Table 6 Response optimization of the synthesis parameters offered by RSM results (parameters are reported as non-coded level)

Response	Goal	Lower	Target	UAMw parameters					Desirability	Predict response value
				A (W)	B (min)	C (°C)	D (W)	E (min)		
PSD (nm)	Minimize	10	14	564	12.35	28.8	282	13.6	0.9866	15
SSA (nm)	Maximize	2000	2400	811.12	16.237	32.446	265.45	10	1.0000	2588

represents the levels of the synthesis parameters as well as the obtained properties of the samples. Figure 18 shows the XRD patterns of the Ta–MOF samples synthesized in different conditions of the UAMw method. The sample ***d***, which was synthesized under optimal conditions, had the peaks related to the formation of Ta–MOF. Presence of the broad peaks indicated the small size of the crystals in this sample. In the samples ***g*** and ***h***, due to the high intensity of the synthesis parameters and destruction of the bonds, some of the XRD patterns of these samples were not formed compared to the optimal sample. In the samples ***e, a, c, b*** and ***f***, although the XRD patterns of Ta–MOF were formed properly, their crystal sizes differed depending on the synthesis conditions.

3.8 Optimization parameters

Based on the experimental designs performed by fractional factorial and also the ANOVA results [34, 35], the regression equations obtained for each property of the Ta–MOF samples were as $PSD = 269 + 11.1\ A - 36.7\ B + 33.8\ C + 96.4\ D - 198\ E$ and $SSA = 1239 + 206\ A - 134\ B - 155\ C + 65\ D + 359\ E$ [34]. According to these equations, which related the synthesis parameters to properties of products, the surface plots are designed (Figs. 19, 20). Based on these plots, various values of PSA and SSA of the Ta–MOF samples are theoretically estimated by selecting different values for Mw power (A), Mw duration (B), ultrasonic temperature (C), ultrasonic power (D) and ultrasonic duration (E). Different synthesis parameters and properties of products (which were experimentally obtained) are reported in Table 4. By generalizing the theoretical equations to the experimental results in Table 4, it is concluded that the experimental results are in good agreement with the theoretical data obtained from the regression models under similar conditions. One of the objectives of this study was to synthesis Ta–MOF samples with ideal properties. Thus, based on the design of the experiments and ANOVA results, RSM was used to achieve the best experimental conditions in order to synthesis products with unique properties (Fig. 21) [36, 37]. Different conditions of UAMw parameters for the production of the Ta–MOF samples with small PSD and high SSA (predicted by RSM) are presented in Table 6.

4 Conclusion

In this study, UAMw was used as a novel method for the facile synthesis of a new Ta–MOF nanomaterial. Since the compounds that were manufactured in this route had ideal properties, UAMw can be used as a new synthesis protocol for the production of a variety of nanostructures. The results showed that synthesis parameters play a major role in the production of Ta–MOF nanostructure with various structures and different physico-chemical properties including PSD of 15 nm and high SSA of 2588 m^2/g. For the systematic study of the parameters on various properties of the Ta–MOF samples as well as optimization of the productions with different properties, the fractional factorial design was used.

Acknowledgements The authors would like to acknowledge financial support for this work from the Shahid Bahonar University of Kerman (Iran).

References

1. C. McKinstry, R.J. Cathcart, E.J. Cussen, A.J. Fletcher, S.V. Patwardhan, J. Sefcik, Scalable continuous solvothermal synthesis of metal organic framework (MOF-5) crystals. Chem. Eng. J. **285**, 718–725 (2016)
2. G. Sargazi, D. Afzali, A. Ghafainazari, H. Saravani, Rapid synthesis of cobalt metal organic framework. J. Inorg. Organomet. Polym. Mater. **24**, 786–790 (2014)
3. Y. Jiang, X. Zhang, X. Dai, W. Zhang, Q. Sheng, H. Zhuo, Y. Xiao, H. Wang, Microwave-assisted synthesis of ultrafine Au nanoparticles immobilized on MOF-199 in high loading as efficient catalysts for a three-component coupling reaction. Nano Res. **10**, 876–889 (2017)
4. A. Nikseresht, A. Daniyali, M. Ali-Mohammadi, A. Afzalinia, A. Mirzaie, Ultrasound-assisted biodiesel production by a novel composite of Fe (III)-based MOF and phosphotangestic acid as efficient and reusable catalyst. Ultrason. Sonochem. **37**, 203–207 (2017)
5. N.A. Khan, S.H. Jhung, Synthesis of metal-organic frameworks (MOFs) with microwave or ultrasound: Rapid reaction, phase-selectivity, and size reduction. Coord. Chem. Rev. **285**, 11–23 (2015)
6. M.R. Armstrong, S. Senthilnathan, C.J. Balzer, B. Shan, L. Chen, B. Mu, Particle size studies to reveal crystallization mechanisms of the metal organic framework HKUST-1 during sonochemical synthesis. Ultrason. Sonochem. **34**, 365–370 (2017)
7. P. George, N.R. Dhabarde, P. Chowdhury, Rapid synthesis of titanium based metal organic framework (MIL-125) via microwave route and its performance evaluation in photocatalysis. Mater. Lett. **186**, 151–154 (2017)
8. S. Kitagawa, Metal–organic frameworks (MOFs). Chem. Soc. Rev. **43**, 5415–5418 (2014)
9. G. Sargazi, D. Afzali, A. Mostafavi, S.Y. Ebrahimipour, Ultrasound-assisted facile synthesis of a new tantalum (V) metal-organic framework nanostructure: design, characterization, systematic study, and CO 2 adsorption performance. J. Solid State Chem. **250**, 32–48 (2017)
10. N.D. Burrows, S. Harvey, F.A. Idesis, C.J. Murphy, Understanding the seed-mediated growth of gold nanorods through a fractional factorial design of experiments. Langmuir **33**, 1891–1907 (2017)
11. G. Maurin, C. Serre, A. Cooper, G. Férey, The new age of MOFs and of their porous-related solids Chem. Soc. Rev. **46**, 3104–3107 (2017)
12. K.K. Gangu, S. Maddila, S.B. Mukkamala, S.B. Jonnalagadda, A review on contemporary metal–organic framework materials. Inorg. Chim. Acta **446**, 61–74 (2016)
13. L. Xu, H. Gong, L. Deng, F. Long, Y. Gu, J. Guan, Complex-mediated synthesis of tantalum oxyfluoride hierarchical nanostructures for highly efficient photocatalytic hydrogen evolution. ACS Appl. Mater. Interfaces **8**, 9395–9404 (2016)
14. G. Sargazi, D. Afzali, N. Daldosso, H. Kazemian, N. Chauhan, Z. Sadeghian, T. Tajerian, A. Ghafarinazari, M. Mozafari, A systematic study on the use of ultrasound energy for the synthesis of nickel–metal organic framework compounds. Ultrason. Sonochem. **27**, 395–402 (2015)
15. H. Fazelirad, M. Ranjbar, M.A. Taher, G. Sargazi, Preparation of magnetic multi-walled carbon nanotubes for an efficient adsorption and spectrophotometric determination of amoxicillin. J. Ind. Eng. Chem. **21**, 889–892 (2015)
16. I. Obot, D. Macdonald, Z. Gasem, Density functional theory (DFT) as a powerful tool for designing new organic corrosion inhibitors. Part 1: an overview. Corros. Sci. **99**, 1–30 (2015)
17. X. Liu, J. Xiong, L. Liang, Investigation of pore structure and fractal characteristics of organic-rich Yanchang formation shale in central China by nitrogen adsorption/desorption analysis. J. Nat. Gas Sci. Eng. **22**, 62–72 (2015)
18. N. Santhosh, G. Radhakrishnamacharya, A.J. Chamkha, Flow of a Jeffrey fluid through a porous medium in narrow tubes. J. Porous Media **18**, 71–78 (2015)
19. L. Esrafili, A.A. Tehrani, A. Morsali, Ultrasonic assisted synthesis of two urea functionalized metal organic frameworks for phenol sensing: a comparative study. Ultrason. Sonochem. **39**, 307–312 (2017)
20. G. Sargazi, D. Afzali, A. Mostafavi, A novel synthesis of a new thorium (IV) metal organic framework nanostructure with well controllable procedure through ultrasound assisted reverse micelle method. Ultrason. Sonochem. **41**, 234–251 (2017)
21. M.-H. Pham, G.-T. Vuong, F.-G. Fontaine, T.-O. Do, Rational Synthesis of metal–organic framework nanocubes and nanosheets using selective modulators and their morphology-dependent gas-sorption properties. Cryst. Growth Des. **12**, 3091–3095 (2012)
22. J.F.S. do Nascimento, B.S. Barros, J. Kulesza, J.B.L. de Oliveira, A.K.P. Leite, R.S. de Oliveira, Influence of synthesis time on the microstructure and photophysical properties of Gd-MOFs doped with Eu+. Mater. Chem. Phys. **190**, 166–174 (2017)
23. D. Chen, C. Chen, W. Shen, H. Quan, S. Chen, S. Xie, X. Luo, L. Guo, MOF-derived magnetic porous carbon-based sorbent: synthesis, characterization, and adsorption behavior of organic micropollutants. Adv. Powder Technol. **28**, 1769–1779 (2017)
24. W.P. Deleu, I. Stassen, D. Jonckheere, R. Ameloot, D.E. De Vos, Waste PET (bottles) as a resource or substrate for MOF synthesis. J. Mater. Chem A **4**, 9519–9525 (2016)
25. J.-C. Yin, T.-Z. Qin, C. Hu, G.-M. He, B.-W. Zhao, C. Zhang, J. Wang, A copper(II)–gadolinium(III) heterometallic MOF: synthesis, structure, and electrochemical property. Mater. Lett. **197**, 221–223 (2017)
26. F. Jeremias, S.K. Henninger, C. Janiak, Ambient pressure synthesis of MIL-100 (Fe) MOF from homogeneous solution using a redox pathway. Dalton Trans. **45**, 8637–8644 (2016)
27. G. Sargazi, D. Afzali, A. Mostafavi, S.Y. Ebrahimipour, Synthesis of CS/PVA biodegradable composite nanofibers as a microporous material with well controllable procedure through electrospinning.

J. Polym. Environ. (2017). https://doi.org/10.1007/s10924-017-1080-8
28. V.K. Vankanti, V. Ganta, Optimization of process parameters in drilling of GFRP composite using Taguchi method. J. Mater. Res. Technol. **3**, 35–41 (2014)
29. Y. Hu, H. Yu, K. Dong, S. Yang, X. Ye, S. Chen, Analysis of the tenderisation of jumbo squid (*Dosidicus gigas*) meat by ultrasonic treatment using response surface methodology. Food Chem. **160**, 219–225 (2014)
30. C. Camposeco-Negrete, Optimization of cutting parameters for minimizing energy consumption in turning of AISI 6061 T6 using Taguchi methodology and ANOVA. J. Clean. Prod. **53**, 195–203 (2013)
31. W. Wang, Q. Li, Y. Liu, B. Chen, Ionic liquid-aqueous solution ultrasonic-assisted extraction of three kinds of alkaloids from Phellodendron amurense Rupr and optimize conditions use response surface. Ultrason. Sonochem. **24**, 13–18 (2015)
32. W. Li, G. Li, Q. Lv, W. Xu, L. Liu, Chromate adsorption on amine-functionalized core/shell magnetic mesoporous material. J. Porous Mater. **22**, 965–972 (2015)
33. Z.-M. Cui, J. Hao, C.-Y. Cao, W. Song, Mesoporous silica (meso-SiO_2) was coated on the micro/nanomaterials with hierarchical structure such as flowerlike Fe_2O_3, flowerlike MgO, SnO_2 nanospheres, Co_3O_4 nanosheets and nanowires from a simple solution method. The structure of the nanomaterials and the silica coating before and after stirring in solution were characterizated by SEM and TEM. The results show that meso-SiO_2 coating was an ideal. J. Porous Mater. **24**, 103–108 (2017)
34. M. Ghaedi, M. Rahimi, A. Ghaedi, I. Tyagi, S. Agarwal, V.K. Gupta, Application of least squares support vector regression and linear multiple regression for modeling removal of methyl orange onto tin oxide nanoparticles loaded on activated carbon and activated carbon prepared from Pistacia atlantica wood. J. Colloid Interface Sci. **461**, 425–434 (2016)
35. D. Liu, C. Huang, J. Wang, H. Zhu, P. Yao, Z. Liu, Modeling and optimization of operating parameters for abrasive waterjet turning alumina ceramics using response surface methodology combined with Box–Behnken design. Ceram. Int. **40**, 7899–7908 (2014)
36. V.K. Gupta, S. Agarwal, M. Asif, A. Fakhri, N. Sadeghi, Application of response surface methodology to optimize the adsorption performance of a magnetic graphene oxide nanocomposite adsorbent for removal of methadone from the environment. J. Colloid Interface Sci. **497**, 193–200 (2017)
37. E. Bet-Moushoul, Y. Mansourpanah, K. Farhadi, M. Tabatabaei, TiO_2 nanocomposite based polymeric membranes: a review on performance improvement for various applications in chemical engineering processes. Chem. Eng. J. **283**, 29–46 (2016)